# Hierarchical Control of Inerter-Enhanced MRD Seat Suspension ⋆

**Xiaohui Yu** * **Xinze Yu** * **Shuyou Yu** * **Jun Yang** * **Hong Chen** **

* *Department of Control Science and Engineering Jilin University, Changchun,China(e-mail: yuxiaohui@jlu.edu.cn).*
** *College of Electronics and Information Engineering Tongji University,Shanghai,China(e-mail: chenhong2019@tongji.edu.cn)*

**Abstract:** Low-frequency vibrations significantly affect ride comfort, yet conventional seat suspensions struggle to suppress them. This paper proposes a novel parallel seat suspension combining a spring, MRD, and inerter, with the inerter optimized for low-frequency isolation. A hierarchical control framework is developed: The lower layer first develops a recurrent neural network (RNN) to capture the MRD's complex dynamics. Subsequently, the Koopman operator framework is applied to construct a lifted linear representation of this data-driven RNN model, enabling accurate force tracking, while the upper layer employs an $H_\infty$ output-feedback controller balancing comfort and robustness. Simulations demonstrate substantial improvements in force tracking and comfort-related metrics, providing a systematic simulation-based framework for robust semi-active seat suspension control.

*Keywords:* Seat Suspension, Magnetorheological Damper (MRD), Inerter, Hierarchical Control.

## 1. INTRODUCTION

Ride comfort is a critical aspect of vehicle design, as low-frequency vibrations are strongly perceived by the human body and contribute to discomfort and fatigue Gillespie (1992). Conventional passive seat suspensions, relying on fixed-coefficient springs and dampers, are constrained by the trade-off between comfort and handling, thus failing to provide adequate isolation in the low-frequency range.

Semi-active suspensions offer a practical compromise, achieving performance close to fully active systems while maintaining lower cost and power consumption. Magnetorheological dampers (MRDs) have been extensively applied in this context owing to their rapid response, low energy requirements, and continuously variable damping characteristics Spencer Jr. et al. (1997). Control strategies such as the Skyhook algorithm Karnopp et al. (1974) have been widely investigated; however, they depend on simplified linearized models and cannot fully exploit the nonlinear hysteretic dynamics of MRDs for optimal vibration attenuation.

Nevertheless, two fundamental challenges persist. First, suspension topology inherently limits low-frequency isolation capability. The inerter, a two-terminal mechanical element that generates force proportional to relative acceleration Smith (2002), presents new opportunities to reshape system dynamics. Its integration with MRDs has shown potential benefits for ride comfort enhancement Yang et al. (2021), yet the mechanism and control optimization require further investigation. Second, while advanced controllers such as $H_\infty$ control can effectively balance comfort and robustness, their overall success hinges on accurate force tracking by the actuator. The nonlinear and hysteretic behavior of MRDs Wang and Liao (2011) introduces notable discrepancies between commanded and realized forces, thereby degrading control performance.

To address these issues, this paper proposes a hierarchical control framework for an inerter-enhanced MRD seat suspension system. The main contributions are: (i) a parallel seat suspension topology combining a spring, MRD, and inerter, with the inertance optimally sized via a genetic algorithm targeting the 0–5 Hz band, achieving a 57.95% reduction in integrated acceleration PSD compared to the conventional passive suspension; and (ii) a two-layer control structure decoupling vibration suppression from actuator compensation, where the lower layer trains an RNN to capture MRD hysteresis and applies Koopman operator theory to obtain a lifted linear approximation for force-tracking controller synthesis. The present work is a simulation-based study; hardware validation is planned as future work.

The remainder is organized as follows: Section 2 presents the system modeling, Section 3 details the hierarchical controller design, Section 4 discusses simulation results, and Section 5 concludes.

## 2. SYSTEM MODELING AND PROBLEM FORMULATION

### *2.1 Governing Dynamic Equations*

The seat suspension system is represented by the 1-degree-of-freedom (1-DOF) model shown in Fig. 1. The model consists of the sprung mass ($m_s$), representing the occupant, connected to the road via a parallel suspension unit.

⋆ This work is supported by the National Natural Science Foundation of China (No. 62473167) and the Natural Science Foundation of Jilin Province, China (No. 20240402079GH)

This unit includes a spring ($k_s$), the inherent damping of the seat suspension system ($c_s$), an inerter ($b$), and the controllable magnetorheological damper (MRD).

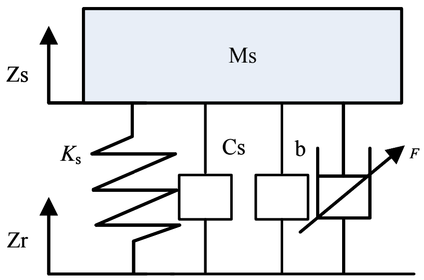


Fig. 1. The 1-DOF seat suspension model (including passive damping $c_s$).

Applying Newton's second law to the sprung mass ($m_s$) yields the governing equation of motion:

$$m_s\ddot{z}_s = -k_s(z_s - z_r) - c_s(\dot{z}_s - \dot{z}_r) - b(\ddot{z}_s - \ddot{z}_r) - F \quad (1)$$

where $z_s$ is the vertical displacement of the sprung mass, $z_r$ is the vertical displacement of the road (which acts as the base excitation), and $F$ is the controllable force generated by the MRD.

### *2.2 Inerter Parameter Optimization*

The value of the inertance, $b$, critically influences the low-frequency dynamics of the suspension system. To maximize the benefits of the inerter, particularly in suppressing vibrations within the frequency range most sensitive to the human body, a Genetic Algorithm (GA) is employed to optimize this parameter.

A GA was adopted as a derivative-free optimizer because the objective is evaluated through time-domain simulation followed by PSD integration. Although the present problem is one-dimensional and could also be solved by grid search or other derivative-free methods, GA provides a convenient and extensible framework for future multi-parameter tuning of $k_s$, $c_s$, and $b$. In this work, GA is used primarily as a practical optimization tool rather than as a theoretically indispensable choice.

The objective function $J_{\text{GA}}(b)$ is defined to approximate the low-frequency vibration energy of the sprung mass (occupant) acceleration $\ddot{z}_s$ within the 0–5 Hz band, evaluated by integrating its power spectral density (PSD) obtained under a sweep-frequency excitation.

$$J_{\text{GA}}(b) = \min_b \left( \int_0^5 \text{PSD}_{\ddot{z}_s}(f, b)\, df \right) \quad (2)$$

where $\text{PSD}_{\ddot{z}_s}(f, b)$ is the power spectral density function of the sprung mass acceleration with respect to frequency $f$ for a given inertance $b$. The input excitation used to drive the system for evaluating this objective function is a sinusoidal sweep signal with an amplitude of 0.01 m, linearly sweeping from 0.01 Hz to 5 Hz. The search space for the GA was set to $[0, 8000]$ kg.

The optimization process successfully identified an optimal inertance value, as illustrated by the PSD comparison in Fig. 2. The resulting optimal value is $b_{\text{opt}} = 28.9$ kg. As shown in Fig. 2, compared to the conventional passive suspension without an inerter ($b = 0$, blue curve), the passive suspension incorporating this optimal inertance ($b = 28.9$ kg, red curve) achieves a significant reduction in the acceleration PSD within the targeted 0–5 Hz optimization band. Quantitative analysis shows that within the broader 0–5 Hz frequency range, the total PSD energy for the optimized suspension is reduced by 57.95% compared to the baseline passive suspension. This optimal value, $b_{\text{opt}} = 28.9$ kg, will be utilized throughout the subsequent controller design and simulation analyses.

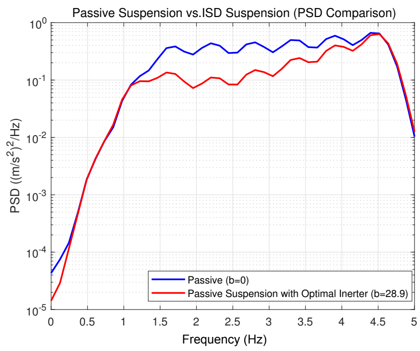


Fig. 2. PSD comparison validating the inerter parameter optimization (Sprung mass acceleration).

### *2.3 Control Objectives*

The primary objective is to enhance ride comfort by attenuating seat vibration while respecting physical constraints. This is challenging because the ideal control force prescribed by any linear control law must be realized by the highly nonlinear magnetorheological (MRD) actuator, necessitating a hierarchical strategy. The high-level objectives guiding the $H_\infty$ controller design (Section 3.2) are: (i) minimize seat vertical acceleration $\ddot{z}_s$ as the primary comfort metric; (ii) constrain suspension travel $z_s - z_r$ within physical limits ($\pm 0.06$ m) to prevent bottoming-out; and (iii) limit control force $u = F$ to remain within the MRD's deliverable range ($\pm 1500$ N).

### *2.4 Dynamic Model of Seat Suspension*

*State-Space Model of Seat Suspension* For the $H_\infty$ controller design, the system described by Eq. (1) is formulated as a generalized plant. We first define the relative state vector:

- State vector ($\mathbf{x}$):
$$\mathbf{x} = [z_{rel}, \dot{z}_{rel}]^T = [z_s - z_r, \dot{z}_s - \dot{z}_r]^T \quad (3)$$
- Disturbance input ($w$): $w = \ddot{z}_r$
- Control input ($u$): $u = F$
- Performance output ($\mathbf{z}$): $\mathbf{z} = [\ddot{z}_s, z_{rel}]^T$

The performance output $\mathbf{z}$ is chosen to capture the two principal trade-offs in suspension design: $\ddot{z}_s$ directly quantifies ride comfort (the primary objective), while $z_{rel} = z_s - z_r$ represents suspension travel, which must be bounded to prevent mechanical interference. This two-output formulation provides the basis for the $H_\infty$ generalized plant developed in Section 3.2, where a third channel for control effort will be appended.

Based on the derivations, the state-space matrices are defined. Let $den = m_s + b$.

$$A = \begin{bmatrix} 0 & 1 \\ -k_s/den & -c_s/den \end{bmatrix} \tag{4}$$

$$B_1 = \begin{bmatrix} 0 \\ -m_s/den \end{bmatrix}, \quad B_2 = \begin{bmatrix} 0 \\ -1/den \end{bmatrix} \tag{5}$$

$$C = \begin{bmatrix} -k_s/den & -c_s/den \\ 1 & 0 \end{bmatrix} \tag{6}$$

$$D_1 = \begin{bmatrix} b/den \\ 0 \end{bmatrix}, \quad D_2 = \begin{bmatrix} -1/den \\ 0 \end{bmatrix} \tag{7}$$

*Data-Driven Modeling and Linearization of Magnetorheological Damper* To precisely capture the complex hysteretic nonlinear dynamics of the MRD, a data-driven approach using a Recurrent Neural Network (RNN), specifically an Elman network, was employed. The network inputs are the instantaneous control current $I(k)$, piston relative displacement $s(k)$, and relative velocity $v(k)$, while the output is the predicted damping force $F(k)$. The network architecture consists of 3 input neurons, 1 output neuron, a single hidden layer with 10 neurons, and a corresponding context layer with 10 neurons. The activation functions chosen were hyperbolic tangent (tanh) for the hidden layer and linear for the output layer. Using 10,000 data points collected from a 2-DOF suspension test rig (at 0.262 m/s max velocity, 0.1A to 1.0A current), the network was trained using the Levenberg-Marquardt algorithm with Mean Squared Error (MSE) as the performance index. The trained RNN model captures the MRD's dynamics with acceptable accuracy on test data, serving as a data-driven surrogate for the subsequent Koopman-based lifted linear approximation. Despite its accuracy, the RNN model's nonlinearity complicates controller design Kim (2020). We apply Koopman operator theory via the Extended Dynamic Mode Decomposition (EDMD) algorithm to construct a lifted linear representation of the trained RNN model itself. The key is selecting appropriate observable functions $\varphi(\mathbf{x}(k))$ to lift the RNN's hidden state $\mathbf{x}(k)$ (a 10-dimensional vector) to a higher-dimensional linear space Xie and Ren (2020). A dictionary of 50 basis functions was constructed: $\varphi_1(\mathbf{x}(k))$ being the RNN's output layer (predicted force); $\varphi_2$ to $\varphi_{40}$ being 39 Gaussian Radial Basis Functions (RBFs) with randomly selected centers; and $\varphi_{41}$ to $\varphi_{50}$ being the 10 hidden states $\mathbf{x}(k)$ themselves. Using data snapshots generated from the RNN, a 50-dimensional discrete-time linear system was identified via least-squares:

$$\boldsymbol{\eta}(k+1) = \mathbf{A}_K\boldsymbol{\eta}(k) + \mathbf{B}_u u_K(k) + \mathbf{B}_d\mathbf{d}(k) \tag{8}$$

$$\hat{y}(k) = \mathbf{C}_K\boldsymbol{\eta}(k) \tag{9}$$

where $\boldsymbol{\eta}(k) = [\varphi_1(\mathbf{x}(k)), \ldots, \varphi_{50}(\mathbf{x}(k))]^T$ is the lifted state vector, $u_K(k) = I(k)$ is the manipulated control current, $\mathbf{d}(k) = [s(k), v(k)]^T$ contains the measured exogenous displacement and velocity signals, and $\hat{y}(k)$ is the predicted damping force. The output matrix is $\mathbf{C}_K = [1, 0, \ldots, 0]$. Although $s(k)$ and $v(k)$ enter the identified Koopman model as measured exogenous signals, the only manipulated variable optimized by the DLQT controller is the coil current $I(k)$. This high-dimensional linear model retains the nonlinear characteristics of the original RNN and is suitable for linear controller design. Note that three different state dimensions appear in this work—the 2-D seat state (Section 2.4.1), the 10-D RNN hidden state, and the 50-D lifted state $\boldsymbol{\eta}(k)$—which operate at distinct hierarchy levels and are not combined into a single state vector. The hierarchical surrogate approach (RNN+Koopman+DLQT) is preferred over direct end-to-end learning because the lifted linear model enables a transparent, analytically derived control law with verifiable properties, whereas a black-box learned controller would require additional validation and safety checks.

## 3. HIERARCHICAL CONTROLLER DESIGN

### *3.1 Overall Control Architecture*

To effectively address the core challenge outlined in the previous section—namely, the discrepancy between the idealized linear suspension model and the highly nonlinear MRD actuator—a hierarchical control framework is designed, as illustrated in Fig. 3.

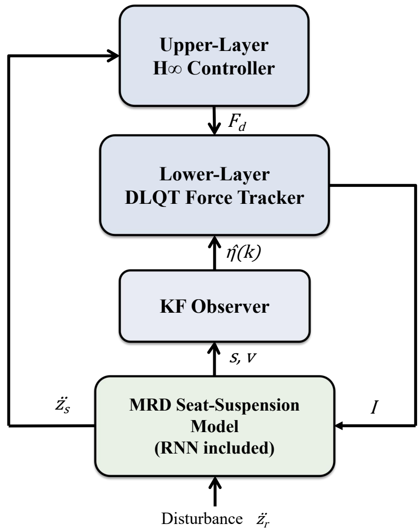


Fig. 3. The proposed hierarchical control architecture, decoupling optimal vibration suppression from nonlinear force tracking.

The framework decouples the control task into two layers: (i) the upper-layer $H_\infty$ controller operates on the linearized seat suspension model, computing an optimal desired damping force $u = F$ from measured $\ddot{z}_s$ for ride comfort and stability, independent of actuator details; (ii) the lower-layer DLQT force tracker takes $F$ as reference and uses the RNN+Koopman model to compute the MRD coil current $I$, compensating for nonlinearity and hysteresis. This decoupling ensures that control performance is not limited by actuator nonlinearities.

### *3.2 Upper-Layer: $H_\infty$ Controller*

$H_\infty$ control minimizes the $H_\infty$-norm $\|T_{zw}\|_\infty$ of the closed-loop transfer function from disturbances $w$ to performance outputs $\mathbf{z}$, providing robust stability and performance against worst-case disturbances Doyle et al. (1989).

Assuming the lower-layer force tracker compensates for MRD nonlinearities, $H_\infty$ control is applied to the linear seat suspension model from Section 2.

*Generalized Plant Formulation and Weighting Functions* The generalized plant $P(s)$ is formulated with the following signals:

- **Disturbance Input ($w$):** The external road acceleration, $w = \ddot{z}_r$.
- **Control Input ($u$):** The desired damping force, $u = F_d$.
- **Measured Output ($y$):** The signal fed back to the controller, selected as the seat acceleration, $y = \ddot{z}_s$.

A static scaling approach is employed. Compared to the two-component output in Section 2.4.1, a third channel $u/U_{max}$ is appended to penalize excessive control effort, following standard $H_\infty$ practice. The performance output $\mathbf{z} = [z_1, z_2, z_3]^T$ is:

$$z_1 = \ddot{z}_s/W_a \tag{10}$$

$$z_2 = (z_s - z_r)/W_t \tag{11}$$

$$z_3 = u/U_{max} \tag{12}$$

where $W_a$, $W_t$, and $U_{max}$ are the constant scaling factors that reflect the control objectives:

(1) **Ride Comfort Weight ($W_a$):** This weight represents the maximum tolerable seat acceleration. A very small value is chosen to strongly penalize acceleration, $W_a = 1.0 \times 10^{-6}$ m/s$^2$.
(2) **Suspension Travel Weight ($W_t$):** This weight defines the maximum allowed suspension travel (rattle space), set to $W_t = 0.06$ m.
(3) **Control Effort Weight ($U_{max}$):** This weight defines the maximum expected control force. The performance output is scaled by this value, $U_{max} = 1500$ N.

These scaling factors are directly embedded within the $C$ and $D$ matrices of the generalized plant $P(s)$.

*Controller Synthesis* With the generalized plant $P(s)$ formulated, the objective of $H_\infty$ control is to find a stabilizing controller $K(s)$ that minimizes the $H_\infty$-norm of the closed-loop transfer function matrix $T_{zw}(s)$ from the disturbance $w$ to the scaled performance output $\mathbf{z}$:

$$\min_{K(s)} \|T_{zw}(s)\|_\infty < \gamma. \tag{13}$$

The resulting controller $K(s)$ is a state-space model characterized by matrices $(A_c, B_c, C_c, D_c)$. It receives the measured seat acceleration $y = \ddot{z}_s$ as input and generates the optimal desired damping force $F_d$ as output, governed by:

$$\dot{\mathbf{x}}_c = A_c\mathbf{x}_c + B_c y, \tag{14}$$

$$u = C_c\mathbf{x}_c + D_c y, \tag{15}$$

where $\mathbf{x}_c$ denotes the internal state vector of the controller.

### *3.3 Lower-Layer: DLQT Force Tracking Controller Design*

Based on the derived high-dimensional discrete-time linear model of the MRD (Eqs. (8)-(9)), a Discrete-time Linear Quadratic Tracker (DLQT) is designed to achieve precise tracking of the desired force $F_d(k)$ Fu and Chen (2022). The DLQT controller finds the optimal control current sequence $u_K(k) = I(k)$ that minimizes the quadratic cost function $J_{\text{DLQT}}$:

$$J_{\text{DLQT}} = \sum_{k=0}^{N-1} \left(\|\hat{y}(k) - F_d(k)\|_Q^2 + \|u_K(k)\|_R^2\right) \tag{16}$$

where $\hat{y}(k) = \mathbf{C}_K\boldsymbol{\eta}(k)$ is the predicted output force. The weighting matrices balance tracking error against control energy: $Q$ is chosen as a diagonal matrix heavily weighting the first element (force error, $10^4$) with other diagonal elements zero, and $R$ is a positive scalar. Solving the discrete-time Riccati equation yields the optimal control law, comprising state feedback and feedforward terms, from which the optimal coil current $I(k)$ is obtained and applied to the MRD.

*Note:* As the lifted state $\boldsymbol{\eta}(k)$ is not directly measurable, a state observer (such as a Kalman Filter) is required in practical implementation to estimate $\boldsymbol{\eta}(k)$.

## 4. SIMULATION RESULTS AND ANALYSIS

Extensive simulations were conducted using MATLAB and Simulink (R2024b) to validate the proposed hierarchical control strategy.

### *4.1 Simulation Setup*

The simulations are based on the 1-DOF seat suspension model established in Section 2. The main parameters of this seat model are listed in Table 1.

Table 1. Simulation Model Parameters (1-DOF Seat)

| Parameter | Value | Unit |
|---|---|---|
| $m_s$ (seat mass) | 75 | kg |
| $k_s$ (seat spring) | 6700 | N/m |
| $c_s$ (passive damping) | 500 | Ns/m |
| $b_{\text{opt}}$ (inerter) | 28.9 | kg |

A key aspect of this study is that the 1-DOF seat model's disturbance input, $w$, is the vehicle chassis acceleration ($\ddot{z}_{\text{chassis}}$), not the raw road profile $z_r$. To generate this realistic chassis vibration, the standard road profiles (described below) were first passed through a separate 2-DOF passive 1/4 vehicle model. The resulting chassis acceleration $\ddot{z}_{\text{chassis}}(t)$ was saved and used as the disturbance input $w(t)$ for all subsequent seat suspension simulations.

The parameters for this 1/4 vehicle "pre-filter" model are listed in Table 2.

Table 2. Parameters of the 1/4 Vehicle Model (Disturbance Generator)

| Parameter | Value | Unit |
|---|---|---|
| $m_{\text{chassis}}$ (Chassis Mass) | 332 | kg |
| $m_{\text{wheel}}$ (Wheel Mass) | 43.5 | kg |
| $k_{\text{susp}}$ (Suspension Spring) | 19800 | N/m |
| $c_{\text{susp}}$ (Suspension Damping) | 3000 | Ns/m |
| $k_{\text{tire}}$ (Tire Spring) | 198000 | N/m |

The two standard road profiles ($z_r$), which were used as the input to the 1/4 vehicle model, are defined as:

(1) **ISO 8608 Class C Random Road Profile:** Simulating driving on an average asphalt road at a speed of 20 m/s. This input is primarily used for the subsequent frequency-domain analysis (PSD).
(2) **Raised-Cosine Bump:** With a height $H = 0.05$ m and length $L = 1$ m, traversed at a speed $v = 10$ m/s. This input is mainly used for the subsequent time-domain transient response analysis.

### 4.2 Force Tracking Performance Validation

The lower-layer force tracker is validated under random road excitation, as shown in Fig. 4.

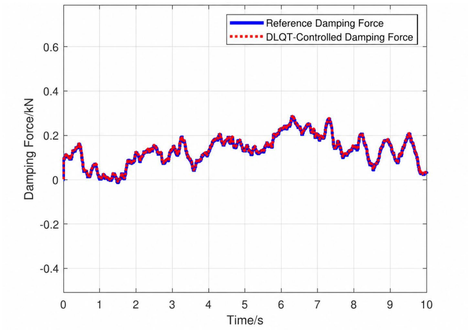


(a) Tracking Performance

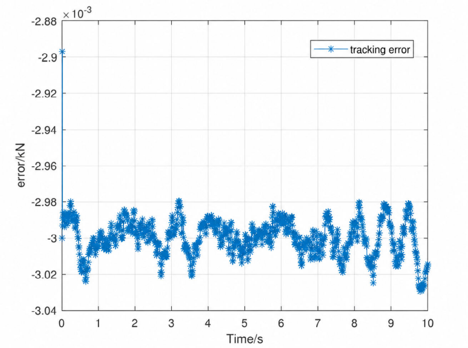


(b) Tracking Error

Fig. 4. Force tracking performance of the lower-layer DLQT controller under random road excitation.

Fig. 4a shows that the actual damping force $F_{mrd}$ (dashed red) closely follows the desired force $F_d$ (blue). Fig. 4b confirms that the tracking error $F_d - F_{mrd}$ remains well bounded, demonstrating that the lower-layer controller effectively compensates for MRD nonlinearity and hysteresis, transforming the MRD into a responsive force actuator.

### 4.3 Vibration Isolation Performance Comparison

Having validated the effectiveness of the lower-layer force tracker, we now evaluate the final performance of the overall hierarchical control system in suppressing seat vibrations. The results are compared against the passive suspension baseline with the optimized inerter.

*Time-Domain Analysis* Figure 5 shows the transient responses of the system when passing over the bump defined in Section 4.1. The figure compares the seat vertical acceleration and the suspension travel for both strategies.

As seen in the seat acceleration subplot (Fig. 5a), the hierarchical control strategy (red curve) demonstrates superior transient performance compared to the passive inerter-based system (blue curve). While the passive system (blue curve) oscillates multiple times before settling around 1.5

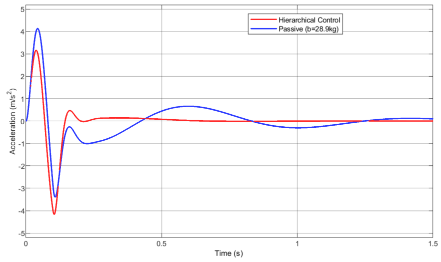


(a) Seat acceleration

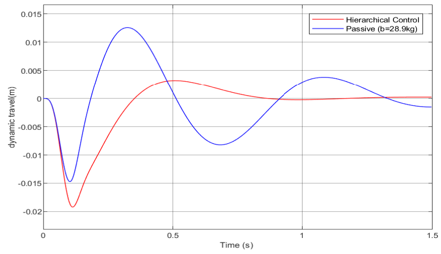


(b) Suspension travel

Fig. 5. Transient response comparison under bump excitation.

seconds, the control strategy achieves the fastest possible vibration attenuation, bringing the system to a near-complete stop in under 0.7 seconds. To quantify the overall performance of this transient event, the Root Mean Square (RMS) value of the seat acceleration was calculated. The proposed hierarchical control strategy reduces the acceleration RMS value by 14.9% compared to the passive inerter-based system, indicating excellent transient ride comfort.

Meanwhile, the suspension travel subplot (Fig. 5b) confirms that the relative displacement remains within the predefined physical limits ($\pm 0.06$ m) for both strategies, satisfying the safety constraint.

*Frequency-Domain Analysis* To assess the steady-state vibration isolation performance under continuous random excitation, particularly in the low-frequency range, we analyze the Power Spectral Densities (PSDs) of the seat vertical acceleration under ISO Class C random road input. The results are presented in Fig. 6.

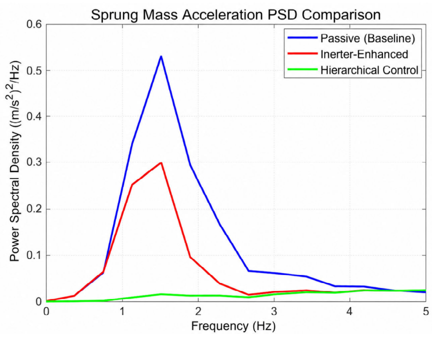


Fig. 6. Comparison of seat acceleration PSD under random road excitation.

The conventional passive suspension shows high PSD in the 0–5 Hz band (integral: 0.6438). The optimized inerter alone reduces this to 0.3463 (46.2% improvement). The proposed hierarchical strategy further reduces it to

0.0716 (88.9% reduction vs. baseline), demonstrating that combining hardware optimization with hierarchical control yields exceptional low-frequency ride comfort improvement.

### *4.4 Summary of Performance Indices*

To provide a clear quantitative comparison of the different control strategies, Table 3 summarizes the root-mean-square (RMS) values of key performance indices under ISO Class C random road excitation.

Table 3. RMS Performance Indices under Random Road Excitation

| Control Strategy | Seat Accel. ($m/s^2$) | Susp. Travel (m) | Base Accel. ($m/s^2$) |
|---|---|---|---|
| Passive ($b = 0$) | 0.8711 | 0.0074 | 1.599 |
| Passive ($b = b_{opt}$) | 0.7106 | 0.0068 | 1.599 |
| Hierarchical Control | 0.4449 | 0.015 | 1.599 |
| Improvement vs. Passive ($b = 0$) | 48.93% | | |

The proposed hierarchical control reduces seat acceleration RMS by 48.93% versus baseline. The passive with optimized inerter achieves 18.5% reduction, validating the parameter optimization. Suspension travel RMS stays within limits for all strategies, and base acceleration change is small, confirming ride comfort gains without stability degradation. These results substantiate the effectiveness of combining inerter optimization with hierarchical control.

## 5. CONCLUSION

This paper presented an integrated solution for low-frequency vibration suppression in seat suspensions. An inerter-enhanced MRD suspension was developed, with inertance optimized via GA. A hierarchical controller was proposed: the lower layer employs an RNN-based Koopman lifted linear model with DLQT for precise force tracking, while the upper layer uses $H_\infty$ control for optimal vibration suppression. Simulations showed 57.95% PSD reduction from inerter optimization alone and 48.93% RMS acceleration reduction with the full hierarchical strategy, while satisfying suspension travel constraints. Future work will focus on hardware-in-the-loop validation and multi-parameter optimization.

## REFERENCES


Doyle, J., Glover, K., Khargonekar, P., and Francis, B. (1989). State-space solutions to standard $H_2$ and $H_\infty$ control problems. *IEEE Transactions on Automatic Control*, 34(8), 831–847.

Fu, Y. and Chen, W. (2022). Optimal tracking control method for discrete-time linear multivariable systems with decoupling performance. *Acta Automatica Sinica*, 48(8), 1931–1939.

Gillespie, T.D. (1992). *Fundamentals of Vehicle Dynamics*. Society of Automotive Engineers, Warrendale, PA.

Karnopp, D., Crosby, M.J., and Harwood, R.A. (1974). Vibration control using semi-active force generators. *Journal of Engineering for Industry*, 96(2), 619–626. doi: 10.1115/1.3438373.

Kim, H. (2020). Development of seismic response simulation model for building structures with semi-active control devices using recurrent neural network. *Applied Sciences*, 10(11), 3915.

Smith, M.C. (2002). Synthesis of mechanical networks: The inerter. *IEEE Transactions on Automatic Control*, 47(10), 1648–1662. doi:10.1109/TAC.2002.803532.

Spencer Jr., B.F., Dyke, S.J., Sain, M.K., and Carlson, J.D. (1997). Phenomenological model of a magnetorheological damper. *Journal of Engineering Mechanics*, 123(3), 230–238. doi:10.1061/(ASCE)0733-9399(1997)123:3(230).

Wang, D. and Liao, W.H. (2011). Mr fluid dampers: a review of parametric modelling. *Smart Materials and Structures*, 20(2), 023001. doi:10.1088/0964-1726/20/2/023001.

Xie, S. and Ren, J. (2020). Linearization of recurrent-neural-network-based models for predictive control of nano-positioning systems using data-driven koopman operators. *IEEE Access*, 8, 147077–147088.

Yang, J., Ning, D., Sun, S., Zheng, J., Lu, H., Nakano, M., Zhang, S., Du, H., and Li, W. (2021). A semi-active suspension using a magnetorheological damper with nonlinear negative-stiffness component. *Mechanical Systems and Signal Processing*, 147, 107071. doi: 10.1016/j.ymssp.2020.107071.